A Model for Unsteady Analysis of Preform Drawing

A model is introduced for analyzing diameter variations occurring in glass fibers drawn from preforms. The heat transfer is shown to be radiation-dominated, and approximate expressions for radiative exchange are developed. The expressions are used in the one-dimensional governing equations for extensional flows to derive a set of linearized disturbance equations. Susceptibility to the draw-resonance instability is determined by solving the disturbance equations as an eigenvalue problem. The sensitivity to an oscillatory take-up rate is also studied as a boundary-value problem. Calculated amplitudes of final diameter perturbations are found to agree well with experimental values.

Matthew R. Myers
Research and Development Laboratory
Corning Glass Works
Corning, NY 14830

Introduction

In the manufacture of fibers and other optical components, precise diameter control is critical to the performance of the product. Variations in fiber diameter can result from an instability of the draw-down flow. Unsteady feed-in rates, heat sources, or take-up speeds will also lead to perturbations to the steady flow and ultimately to diameter nonuniformities. It is of significant interest to quantify the sources of diameter variations for a given set of operating conditions.

Of particular interest here is preform drawing, wherein fibers are produced by applying tension to the bottom of a glass rod as it is lowered into a furnace. Due to the close proximity of the furnace wall, estimates of convective heat transfer based upon boundary layer theories are not applicable. A scaling of variables which includes furnace dimensions and temperatures reveals that radiation is the dominant form of heat transfer in preform drawing.

Models of viscous draw-down flows are typically based upon a "quasi-one-dimensional" approximation, in which the spatial dependence of the axial velocity, pressure, and temperature is entirely in the axial direction. Glicksman (1968) derived the one-dimensional equations for steady-state glass flows. Kase and Matsuo (1965) developed the time-dependent, one-dimensional equations appropriate for polymer spinning and obtained steady-state solutions to them.

Studies of unsteady fiber drawing have included numerous treatments of isothermal flows. Pearson and Matovich (1969) calculated the diameter response to unsteady boundary conditions. Gelder (1971), with linear stability theory, explained the resonant responses obtained by Pearson and Matovich. Ishihara and Kase (1975), Fisher and Denn (1975), and Schultz et al. (1984) performed nonlinear analyses of this "draw-resonance" instability. These investigations showed that viscous-dominated, isothermal extensional flows become unstable when the extension ratio (ratio of final to initial fiber velocity) exceeds the relatively small value of 20.21.

The linear stability of nonisothermal drawing has been studied by Shah and Pearson (1972a,b), Kase (1974), Pearson and Shah 1974), Pearson et al. (1976), Fisher and Denn (1977), and Mhaskar and Shah (1977). [See the review articles by Petrie and Denn (1976) and Denn (1980) for a more comprehensive list.] In all of these analyses, it was assumed that the total heat transferred from the fiber was proportional to a heat transfer coefficient times the fiber temperature measured above an ambient temperature. It was found that stability was greatly enhanced (i.e., the critical extension ratio increased significantly) as the heat transfer capability increased.

From a practical standpoint, the stability of a draw-down process is usually of less concern than its sensitivity to small external disturbances. Kase and Matsuo (1967) calculated the fiber area response to an abrupt increase in cooling air velocity. Kase and Araki (1982) and Young and Denn (1988) determined the frequency response to a variety of disturbances, including take-up speed, spinneret temperature, and extrusion speed. Other sensitivity studies are documented in Denn (1980).

Due to the absence of a radiative-heat-transfer model, the above nonisothermal investigations apply primarily to extrusion processes, wherein the fiber is pulled into air from an orifice. Geyling and Homsy (1980) account for radiation transfer by allowing exchange with an effective farfield temperature which

varies in the axial direction. The configuration factor between the glass surface and the furnace wall is not taken into account, nor is the variation of emissivity with glass radius. In their analysis of steady flows Paek and Runk (1978) account for the neck-down shape in the calculation of radiation heat transfer. However, their expression becomes singular as the preform radius approaches the furnace radius (an important limit in practice.) As far as the author is aware, the expression has not been corrected.

In order to obtain quantitative information about diameter variations arising in preform-drawing processes, it was necessary to construct a model which systematically includes the important components of radiation heat transfer. In this paper a radiation model is developed which accounts for the shape of the preform, the variation in emissivity with preform radius, and the spectral dependence of glass properties. A set of mean and linearized disturbance equations is derived by inserting the model into the one-dimensional equations of motion. The disturbance equations are solved as an eigenvalue problem to determine the susceptibility of the flow to the draw-resonance instability. The sensitivity to an unsteady take-up rate is analyzed as a boundary value problem, and the results are compared with experimental values.

Silica glass properties are used whenever specification is necessary, though extension of the theory to include other types of glasses is straightforward.

Governing Equations

Consider a glass preform of initial radius R_0 inside of a furnace liner of radius b, as shown in Figure 1. The liner extends from $z = 0$ to $z = L$, where the positive z axis extends downward and coincides with the axis of rotation of the system. Between the glass and the wall there is often a flow of purge gas to prevent combustion.

The temperature profile of the liner (discussed further in the next section) has the form displayed to the right in Figure 1. The maximum of the profile is only slightly (roughly 20% in absolute temperature) higher than the softening point T_s. As the preform descends its temperature increases until it reaches T_s at the location z_0. At this point the preform begins to contract under tension. The radius of the elongating preform as a function of axial position is denoted by $R(z)$. The melt cools after it passes the hottest part of the furnace; at coordinate z_1 the temperature has decreased to the softening point. In this paper it will be assumed that the glass instantaneously freezes (and unfreezes, during heating) when its temperature reaches T_s.

If the molten glass jet is slender, i.e., if the initial radius of the jet is small compared to the draw-down length, the full equations of motion can be approximated by a set of quasi-one-dimensional equations. In the one-dimensional model, the pressure, axial velocity, and temperature depend only on the axial coordinate and time. Under isothermal conditions, Schultz and Davis (1982) derived the one-dimensional equations of motion as the leading-order equations in an asymptotic expansion based upon the jet slenderness ratio. A similar analysis under nonisothermal conditions requires consideration of the full integro-differential equations of heat transfer, and hence is considerably more difficult. Here we rely on the experimental evidence of Geyling and Homsy (1980) to justify the one-dimensional assumption for preform drawing. We assume that inertia, gravity, and surface tension are negligible in relation to the viscous stress, though the nonviscous forces can be incorporated with no conceptual difficulty. The viscous-dominated assumption is satisfied in typical preform-drawing operations. The governing equations are well known (for example, Glicksman, 1968) and can be easily derived by performing a mass, momentum, and energy balance on a cylindrical control volume of small axial extent. The equations for a Newtonian fluid are:

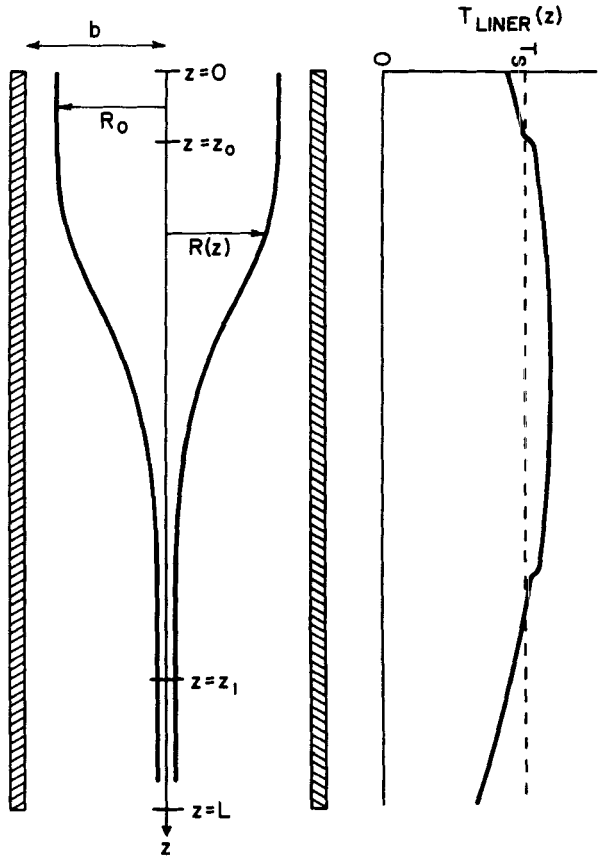

Figure 1. Cross-sectional view of preform-drawing system.
Temperature profile of furnace liner is shown at the right.

Continuity:

$$\frac{\partial}{\partial t}(R^2) + \frac{\partial}{\partial z}(R^2 v_z) = 0. \tag{1}$$

Momentum:

$$\mu R \frac{\partial^2 v_z}{\partial z^2} + 2\mu \frac{\partial R}{\partial z}\frac{\partial v_z}{\partial z} + R\frac{\partial v_z}{\partial z}\frac{\partial \mu}{\partial z} = 0. \tag{2}$$

Energy:

$$\rho c_p \pi R^2 \left(\frac{\partial T}{\partial t} + v_z \frac{\partial T}{\partial z}\right) = \frac{\partial}{\partial z}\left(k\pi R^2 \frac{\partial T}{\partial z}\right) - 2\pi R(q_e - q_a + q_c). \tag{3}$$

Boundary Conditions:

At $z = z_0$:

$$R = R_0 \tag{4a}$$

$$v_z = V_0 \tag{4b}$$

$$T = T_s. \tag{4c}$$

At $z = z_1$:

$$v_z = V_1 \tag{4d}$$

$$T = T_s. \tag{4e}$$

where

t = time

$R(z, t)$ = radius of the jet

$T(z, t)$ = temperature

$v_z(z, t)$ = axial velocity

The relevant glass properties are the thermal conductivity, k, the density, ρ, the specific heat, c_p, and the viscosity, μ, which is a strong function of T. The terms, q_e and q_a, are the emitted and absorbed radiative energy per unit area, and q_c represents the convective heat transfer to the surrounding gas. The various forms of heat transfer will be considered further.

The ability of the glass to transfer heat to the surrounding purge gas is determined by the velocity and thermal properties of the gas. The proper scaling of this convective heat transfer can be determined in the following way. For the purge gas inside the draw-down zone, the ratio of the amount of energy convected in the axial direction to the heat which diffuses between the glass surface and the furnace wall is $\mathrm{E}^2 RePr$, where Re is the Reynolds number based on L, Pr is the Prandtl number, and $\mathrm{E} = b/L$ measures the slenderness ratio of the glass jet. Order-of-magnitude estimates for Re, Pr, and ϵ are 100, 1, and 0.1, making the above product of order unity. Thus, convection and diffusion of temperature are comparable; no boundary layer exists on the surface of the fiber. The convective heat transfer from the glass to the air,

$$-k_{\text{gas}} \frac{\partial T}{\partial r}, \tag{5a}$$

then scales as

$$\frac{k_{\text{gas}} \Delta T_r}{b}, \tag{5b}$$

where ΔT_r is a representative temperature difference between the surface of the glass and the wall. An estimate for ΔT_r is the axial-temperature-difference scale ΔT_z, equal to the difference between the maximum furnace liner temperature and T_s. Note that for extrusion processes ΔT_r is comparable to T_s and the boundary layer thickness is small compared to b, making convective heat transfer much more important than for preform drawing.

The magnitude of the net radiative heat transfer $q_e - q_a$ is of order

$$\sigma(T_{\text{glass}}^4 - T_{\text{wall}}^4) \approx 4\sigma T_s^3 \Delta T_r, \tag{6}$$

where σ is the Stefan-Boltzman constant. By dividing Eq. 5b by Eq. 6, we find that the convective heat transfer is over two orders of magnitude smaller than the radiative heat transfer for T_s = 1,900 K (appropriate for silica glass) and furnace dimensions on the scale of centimeters.

The effect of conduction is likewise small relative to radiative exchange with the furnace, even when a "radiation conductivity" is considered. At high temperatures, radiation conductivity is larger than regular conductivity. The term representing axial conduction of heat in Eq. 3 is of magnitude

$$\mathrm{E}^2 \pi k_r \Delta T_z, \tag{7a}$$

where

$$k_r = \frac{-16 n^2 \sigma T_s^3}{3a}, \tag{7b}$$

and n is the index of refraction and a the absorption coefficient. For silica glass at 2,000°C, the concept of radiation conductivity is valid for wavelengths above 3 μm, where $a \approx 4\ \mathrm{cm}^{-1}$ provides a reasonable estimate. By using this value in Eqs. 7 and comparing with $2\pi b$ times Eq. 6, we see that conduction is weaker than radiation exchange with the wall by at least a factor of E^2.

We have found that, under conditions which prevail in preform-drawing processes, conduction may be neglected along with convective heat transfer to the surrounding gas. A good approximation to the energy equation is then

$$\frac{\partial T}{\partial t} + v_z \frac{\partial T}{\partial z} = -\frac{2}{\rho c_p R}(q_e - q_a). \tag{8}$$

Radiation Model

The assumptions made in the radiation model are the following:

1) The radiation from the glass to the liner does not significantly affect the liner temperature. This assumption is good throughout most of the draw-down zone, since the glass occupies only a small fraction of the furnace volume. In addition, for preform diameters normally used in practice, glass is transparent to much of the radiation emitted by the wall. At 2,000°C silica glass preforms are essentially transparent to over 70% of the blackbody radiation. Hence the temperature of the liner can be decoupled from that of the glass.

2) The furnace liner is a diffuse gray surface. The difficulties associated with measuring high temperatures makes theoretical predictions worth pursuing. When the liner is a diffuse gray surface, and its temperature is essentially decoupled from that of the glass, the temperature and intensity profile can be calculated by the method of Usiskin and Siegel (1960). The axial distribution of heat input into the liner must be known, in addition to the liner emissivity. If the maximum liner temperature is provided the magnitude of the heat distribution need not be specified. In Appendix A we calculate the temperature and intensity profile for a typical industrial furnace with a graphite liner having emissivity 0.75 (see p. 127 of Siegel and Howell, 1981).

3) The directional dependence of the emissivity and absorptivity for the preform is neglected: i.e., the glass is modeled as a diffuse spectral surface. As shown by Gardon (1956) for a glass sheet, this assumption becomes invalid for angles near 90° (where 0 degrees represents the normal). However, for large angles the configuration factor is small and there is little contribution to the total radiative flux. The directional spectral emissivity, ϵ'_λ, and directional spectral absorptivity, α'_λ, are taken to be equal to the hemispherical spectral emissivity, ϵ_λ. Values of the hemispherical spectral emissivity for cylindrical glass media have been estimated by Sayles and Caswell (1981). Their results are reproduced in Figure 2.

The optical thickness referred to in Figure 2 is the product of the fiber diameter times the absorption coefficient at a given wavelength. Unfortunately at temperatures near the softening point of silica glass, values for the absorption coefficient are not well known. Data taken at room temperature is used in this model until high-temperature data become available. The absorption coefficient for glass can usually be closely represented by a step (band) model; such a model for silica glass is given in Figure 3. Once the fiber diameter is specified, the emissivity is calculated from Figures 2 and 3. We remark that when the fiber diameter is above 0.5 cm (roughly), precise values of the absorption coefficient are not required. In this regime the emissivity is effectively zero for wavelengths below about 3 μm, and the asymptotic value 0.9 is attained above 3 μm.

The energy per unit area emitted by an element on the glass surface is

$$q_e = \int e_{\lambda b}\epsilon_\lambda \, d\lambda, \tag{9}$$

where $e_{\lambda b}$ is the blackbody hemispherical spectral emissive power. After incorporating a band model for ϵ_λ, we have

$$q_e = \sum_i \epsilon_{\lambda,i} \int_{\lambda_i}^{\lambda_{i+1}} e_{\lambda b} \, d\lambda. \tag{10}$$

Over each wavelength band the emissivity $\epsilon_{\lambda,i}$ is constant. For the band model of Figure 3, $i = 2$, with $\lambda_1 = 3$ μm, $\lambda_2 = 4.8$ μm, and $\lambda_3 = 8$ μm. The final form for the radiated energy per unit area is obtained by inserting the specific form of the Planck distribution function into $e_{\lambda b}$:

$$q_e = \sigma T^4 \sum_i \epsilon_{\lambda,i} \frac{15}{\pi^4} \int_{\xi_{i+1}}^{\xi_i} \frac{\xi^3}{\exp \xi - 1} \, d\xi, \tag{11a}$$

where

$$\xi_i = 14{,}388 \ \mu\text{m} \cdot \text{K}/\lambda_i T \tag{11b}$$

Because only the limits of integration depend on any of the physical variables, the integral in Eq. 11 can be computed efficiently by interpolating between tabulated values and numerical quadrature is unnecessary.

To calculate the energy per unit area absorbed by the glass, consider a small element of area dA_w on the wall radiating to a small element of area dA_g on the surface of the glass. The energy radiated by dA_w which is absorbed by dA_g is

$$d^2Q_a = \frac{\cos \beta_g \cos \beta_w dA_g dA_w}{S^2} \int_\lambda \alpha'_\lambda i'_{\lambda,w} \, d\lambda, \tag{12}$$

where β_g and β_w are the angles that the normals to dA_g and dA_w make with the vector joining the two areas, S is the distance between dA_g and dA_w, and $i'_{\lambda,w}$ is the spectral intensity of the radiation leaving dA_w. Explicit forms for the geometric quantities are given in Appendix B. The radiation leaving dA_w is composed of reflected as well as emitted radiation. However, since the emissivity of the liner is high (approximatedly 0.75), for the purpose of determining spectral composition we will assume that the radiation is emitted from a gray body at temperature of T_w, with an effective emissivity equal to $U/(\sigma T_w^4)$. Here U is the total energy per unit area leaving dA_w and T_w the local wall temperature. Upon setting the glass absorptivity equal to the emissivity, incorporating the step representation for the emissivity, and

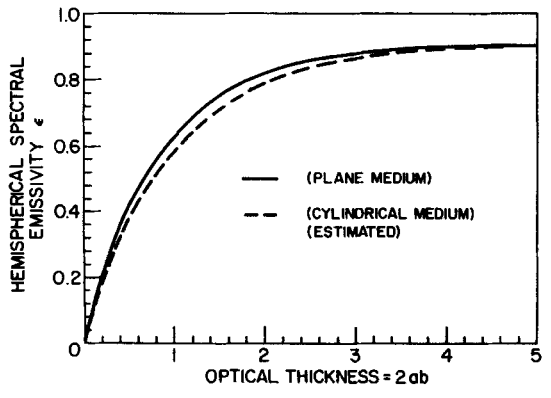

Figure 2. Emissivity as a function of optical thickness.
From Sayles and Caswell (1981)
a = the absorption coefficient; b = the cylinder radius

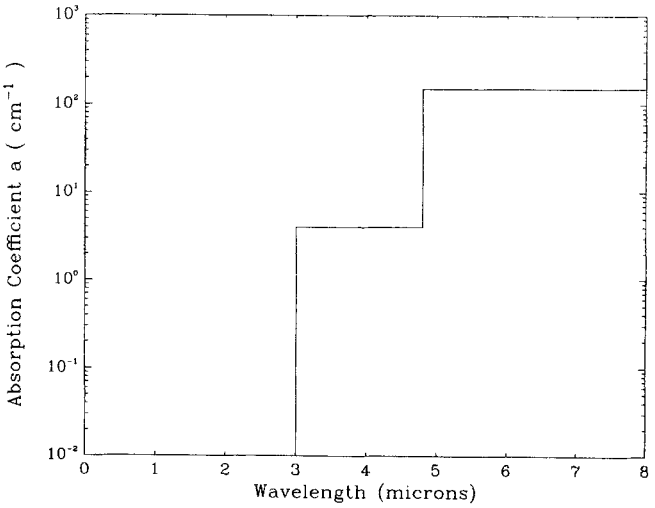

Figure 3. Step model for absorption coefficient of silica glass.
Measured at room temperature by H. Hoover, Corning Glass Works.

writing out the Plank distribution function, we arrive at:

$$d^2Q_a = \frac{\cos\beta_g \cos\beta_w dA_g dA_w}{S^2} \frac{U}{\pi} \sum_i \cdot \epsilon_{\lambda,i} \frac{15}{\pi^4} \int_{\xi_{i+1,w}}^{\xi_{i,w}} \frac{\xi^3}{\exp\xi - 1} d\xi, \quad (13a)$$

where

$$\xi_{i,w} = 14{,}388\ \mu\text{m} \cdot \text{K}/\lambda_i T_w. \quad (13b)$$

To obtain the total radiation absorbed by dA_g due to incident radiation from all parts of the furnace, we must integrate with respect to dA_w. The integration in the circumferential direction can be done in closed form; the result is given in Appendix B. The final result is an integral over the liner in the axial direction:

$$q_a = \frac{\int_{A_w} d^2Q_a}{dA_g} = \int_0^L dz_w U(z_w) F(z, R, z_w) \cdot \sum_i \epsilon_{\lambda,i} \frac{15}{\pi^4} \int_{\xi_{i+1}(z_w)}^{\xi_i(z_w)} \frac{\xi^3}{\exp\xi - 1} d\xi, \quad (14)$$

where z and R are coordinates for dA_g and the geometric factor F is given by Eq. 4 of Appendix B. The temperature used in calculating ξ_i is the local wall temperature at coordinate z_w. The radiative energy per unit area leaving the furnace, $U(z_w)$, and the wall temperature profile, $T_w(z_w)$, are calculated in Appendix A.

Solution Strategy

We first make the following transformations, which nondimensionalize the governing equations and introduce the disturbance variables.

$$z = L\zeta \quad (15a)$$

$$t = \frac{L}{V_0}\tau \quad (15b)$$

$$v_z/V_0 = \bar{\psi}(\zeta)[1 + \psi'(\zeta, \tau)] \quad (15c)$$

$$R/b = \bar{\chi}(\zeta)[1 + \chi'(\zeta, \tau)] \quad (15d)$$

$$T/T_s = \bar{\theta}(\zeta)[1 + \theta'(\zeta, \tau)] \quad (15e)$$

$$q_e = \sigma T_s^4 \phi(\zeta, R/b, T/T_s) \quad (15f)$$

$$q_a = \sigma T_s^4 \phi_a(\zeta, R/b) \quad (15g)$$

$$\mu = \mu(T_s)\eta(T/T_s). \quad (15h)$$

The time-varying quantities are assumed small compared to the mean quantities. We now insert Eqs. 15 into Eqs. 1, 2 and 8, and neglect squares of primed quantities. The mean equations arise at zeroth order in the primed quantities:

$$\frac{d}{d\zeta}(\bar{\chi}^2\bar{\psi}) = 0 \quad (16a)$$

$$\frac{d^2\bar{\psi}}{d\zeta^2} + \frac{2}{\bar{\chi}}\frac{d\bar{\psi}}{d\zeta}\frac{d\bar{\chi}}{d\zeta} + \frac{1}{\eta}\frac{d\eta}{d\bar{\theta}}\frac{d\bar{\theta}}{d\zeta}\frac{d\bar{\psi}}{d\zeta} = 0 \quad (16b)$$

$$\bar{\psi}\frac{d\bar{\theta}}{dz} = -\frac{C_R}{\bar{\chi}}(\phi_e - \phi_a) \quad (16c)$$

where

$$C_R = \frac{2\sigma T_s^3 L}{\rho c_p V_0 b}. \quad (16d)$$

Because of the nondimensionalization by the initial velocity, the radiation transfer coefficient is normally quite large. For silica glass $C_R \approx 150$. Geyling and Homsy (1980) give a range of 0.1 to 2.0 for their radiative transfer coefficient, which is nondimensionalized by room temperature. Scaled on the softening point of silica glass this range becomes about 30 to 600. The velocity typically increases by more than a factor of 100 throughout the elongation process, so that a scaling by the final velocity would produce a coefficient less than (possibly much less than) one. The physical implication is that at the top of the draw-down zone the radiation transfer terms dominate: i.e., the temperature is dictated just by a balance of emitted and absorbed radiation. At the bottom of the draw-down zone the convection of energy down the fiber is more important than heat transfer by radiation.

At first order in the primed quantities we have the linearized disturbance equations:

$$\frac{\partial\chi'}{\partial\tau} + \bar{\psi}\frac{\partial\chi'}{\partial\zeta} + \frac{\bar{\psi}}{2}\frac{\partial\psi'}{\partial\zeta} = 0 \quad (17a)$$

$$\bar{\psi}\frac{\partial^2\psi'}{\partial\zeta^2} + \left(\frac{d\bar{\psi}}{d\zeta} + \frac{1}{\eta}\frac{d\eta}{d\bar{\theta}}\frac{d\bar{\theta}}{d\zeta}\bar{\psi}\right)\frac{\partial\psi'}{\partial\zeta} + 2\frac{d\bar{\psi}}{d\zeta}\frac{\partial\chi'}{\partial\zeta} + \frac{\bar{\theta}}{\eta}\frac{d\bar{\psi}}{d\zeta}\frac{d\eta}{d\bar{\theta}}\frac{\partial\theta'}{\partial\zeta} + \left[\frac{\bar{\theta}}{\eta}\frac{d\bar{\theta}}{d\zeta}\frac{d\bar{\psi}}{d\zeta}\frac{d^2\eta}{d\bar{\theta}^2} + \frac{1}{\eta}\frac{d\eta}{d\bar{\theta}}\frac{d\bar{\theta}}{d\zeta}\frac{d\bar{\psi}}{d\zeta} - \frac{\bar{\theta}}{\eta^2}\frac{d\bar{\theta}}{d\zeta}\frac{d\bar{\psi}}{d\zeta}\left(\frac{d\eta}{d\bar{\theta}}\right)^2\right]\theta' = 0 \quad (17b)$$

$$\bar{\theta}\frac{\partial\theta'}{\partial\tau} + \bar{\theta}\bar{\psi}\frac{\partial\theta'}{\partial\zeta} + \bar{\psi}\frac{d\bar{\theta}}{d\zeta}(\theta' + \psi' + \chi') = -\frac{C_R}{\bar{\chi}}\left(\bar{\chi}\chi'\frac{\partial\phi_e}{\partial\bar{\chi}} + \bar{\theta}\theta'\frac{\partial\phi_e}{\partial\bar{\theta}} - \bar{\chi}\chi'\frac{\partial\phi_a}{\partial\bar{\chi}}\right). \quad (17c)$$

The term $\partial\phi_a/\partial\bar{\chi}$ accounts for the change in configuration factor and glass absorptivity as the fiber radius changes. The factor $\partial\phi_e/\partial\bar{\chi}$ likewise accounts for changes in emissivity with radius, in the emitted radiation. The change in spectral distribution with temperature of the emitted radiation is contained in $\partial\phi_e/\partial\bar{\theta}$. Differentiation of ϕ_a with respect to $\bar{\chi}$ is performed by differentiating through the integral sign in Eq. 14. To avoid numerical differentiation of tabulated values, the points comprising Figure

2 can be closely fit to a function having a negative-exponential form.

In order to solve the mean and disturbance equations it is necessary to specify a viscosity-temperature relation. We choose the following:

$$\mu(T) = \mu(T_s) \exp\left[\gamma\left(\frac{T_s}{T} - 1\right)\right], \tag{18a}$$

for which

$$\frac{1}{\bar{\eta}(\bar{\theta})}\frac{d\bar{\eta}}{d\bar{\theta}} = -\frac{\gamma}{\bar{\theta}^2}. \tag{18b}$$

The relation is based upon empirical data for silica glass, with $\gamma \approx 32$. The viscosity-temperature dependence for other glasses is also quantitatively captured. For the specific viscosity-temperature relation in Eq. 18, the mean and disturbance momentum equations (Eqs. 16B and 17B) become

$$\frac{d^2\bar{\psi}}{d\zeta^2} + \frac{2}{\bar{\chi}}\frac{d\bar{\chi}}{d\zeta}\frac{d\bar{\psi}}{d\zeta} - \frac{\gamma}{\bar{\theta}^2}\frac{d\bar{\theta}}{d\zeta}\frac{d\bar{\psi}}{d\zeta} = 0 \tag{19}$$

and

$$\bar{\psi}\frac{\partial^2\psi'}{\partial\zeta^2} + \left(\frac{d\bar{\psi}}{d\zeta} - \frac{\gamma}{\bar{\theta}^2}\frac{d\bar{\theta}}{d\zeta}\bar{\psi}\right)\frac{\partial\psi'}{\partial\zeta} + 2\frac{d\bar{\psi}}{d\zeta}\frac{\partial\chi'}{\partial\zeta} - \frac{\gamma}{\bar{\theta}}\frac{d\bar{\psi}}{d\zeta}\frac{\partial\theta'}{\partial\zeta} + \frac{\gamma}{\bar{\theta}^2}\frac{d\bar{\theta}}{d\zeta}\frac{d\bar{\psi}}{d\zeta}\theta' = 0. \tag{20}$$

The type of boundary condition imposed depends on the kind of problem under consideration. In this paper we study three kinds, which are described below. Results obtained by numerical solutions of the equations will be discussed later.

Mean (base) flow

Equations 16a, 16c and 19 are solved subject to the following boundary conditions:

$$\bar{\chi}(\zeta_0) = \bar{\chi}_0$$
$$\bar{\psi}(\zeta_0) = 1$$
$$\bar{\theta}(\zeta_0) = 1 \tag{21a}$$
$$\bar{\psi}(\zeta_1) = E \tag{21b}$$
$$\bar{\theta}(\zeta_1) = 1. \tag{21c}$$

where $\zeta_0 = z_0/L$, $\zeta_1 = z_1/L$, $\bar{\chi}_0 = R_0/b$, and $E = V_1/V_0$ is the extension ratio. The endpoints of the draw-down zone, ζ_0 and ζ_1, are a function of the glass radius and must be determined as part of the solution. It was noted earlier that, for large C_R, the energy equation (Eq. 16c) reduces to a balance of emitted and absorbed radiation at the top of the draw-down zone. Thus ζ_0 can be obtained by solving a nonlinear algebraic equation once the radius of the preform at the top is specified. The lower endpoint must be found by solving the differential equation. The solution strategy we adopted was to adjust the values of ζ_1 and $(d\bar{\chi}/d\zeta)(\zeta_0)$ until the solutions of Eqs. 16a, 16c and 19 satisfied Eqs. 21, using a Newton method to refine the iterates. The differential equations were solved with a predictor-corrector method. Computation times were reduced by first calculating the absorbed radiation at specified locations inside the furnace volume, and storing the results in a two-dimensional array. Values of the absorbed radiation required in the solution of the differential equation were then obtained by interpolation. Required CPU time on a VAX8800 was on the order of a minute.

Eigenvalue problems

Normal modes of the form

$$\psi'(\zeta, \tau) = [\psi_r(\zeta) + i\psi_i(\zeta)]e^{(\omega_r + i\omega_i)\tau} \tag{22a}$$

$$\chi'(\zeta, \tau) = [\chi_r(\zeta) + i\chi_i(\zeta)]e^{(\omega_r + i\omega_i)\tau} \tag{22b}$$

$$\theta'(\zeta, \tau) = [\theta_r(\zeta) + i\theta_i(\zeta)]e^{(\omega_r + i\omega_i)\tau} \tag{22c}$$

are assumed, where $i = \sqrt{-1}$. Equations 17a, 17c and 20 are decomposed into real and imaginary parts and solved subject to homogeneous boundary conditions:

$$\chi_r(\zeta_0) = \chi_i(\zeta_0) = \psi_r(\zeta_0) = \psi_i(\zeta_0) = \theta_r(\zeta_0) = \theta_i(\zeta_0) = 0 \tag{23a}$$

$$\psi_r(\zeta_1) = \psi_i(\zeta_1) = 0. \tag{23b}$$

Boundary conditions (Eqs. 23) are only approximate, since they don't account for the shift in melting-point or freezing-point location due to local temperature variations [i.e., nonzero $\theta'(\zeta_0, \tau)$ or $\theta'(\zeta_1, \tau)$]. Pearson, Shah, and Mhaskar (1976) and Chang, Denn, and Kase (1982) derive more realistic "dynamic" boundary conditions, as will be considered below. Pearson, Shah, and Mhaskar also allow for the elasticity of the solid fiber.

For a given extension ratio and draw-down length, the homogeneous system has a solution only for a discrete set of eigenvalues $\{(\omega_r + i\omega_i)_n\}$. The real parts determine the susceptibility of the draw-down flow to the "draw-resonance" instability. The flow is linearly stable if all real parts are negative, as any imposed infinitesimal perturbations decay with time. The flow is linearly unstable if any real part is positive.

Once the base flow is determined, the normal modes can be found by iteration on ω_r and ω_i. Of more interest in this paper, though, is the value of the critical extension ratio as a function of the viscosity-temperature coefficient, γ. The critical extension ratio is the value of E for which the least negative ω_r is zero. Because E is unknown, the mean flow must be solved along with the disturbance flow. The solution strategy employed in the mean flow solution is also applicable here, except that iteration on three variables is required. Processor requirements for our computations were found to be slightly larger than those for the mean-flow solution.

Boundary-value problems

A periodic velocity $\psi_r = e^{i\omega\tau}$ is imposed at ζ_1, which models the effect due to an unsteady take-up rate. Purely oscillatory normal modes at frequency ω are assumed; the modes are given by Eqs. 22 with $\omega_r = 0$ and $\omega_i = \omega$. The boundary conditions are identical to Eqs. 23, except for

$$\psi_r(\zeta_1) = 1. \tag{24}$$

Since the disturbance equations are linear, the amplitude of the forcing velocity may be taken to be unity. The dynamic boundary condition (Pearson et al., 1976; Chang et al., 1982) at ζ_1, in the present notation, is:

$$-\frac{1}{E}\frac{d\bar{\psi}/d\zeta}{d\bar{\theta}/d\zeta}(\theta_r + i\theta_i) + \psi_r + i\psi_i = 1. \qquad (25)$$

The effect of imposing boundary condition (Eq. 25) was assessed in the calculations. A similar dynamic condition could be applied at the melting point ζ_0, whenever a temporal dependence is imposed on the feed-in process. For example, preform roughness will vary the radiation configuration factor and hence the local temperature, causing the melting-point location to shift.

The boundary value problem can be solved by standard shooting methods, in which $d\psi_r/d\zeta$ and $d\psi_i/d\zeta$ at ζ_0 are adjusted until convergence is achieved. Mean flow quantities calculated above are utilized in the solution. The amount of processor time required was again on the order of a minute on a VAX 8800.

Results and Discussion

For all of the results described in this section, the furnace liner described in Appendix A applies. The glass in each case is fused silica.

The model was tested in the case of steady flows by comparing the predicted radius profile with an actual shape. The experimental shape was obtained by measuring the quenched preform remaining after the drawing process. The two radius profiles are displayed in Figure 4. The experimental and theoretical values are seen to agree well, given the limitations of the one-dimensional model. The maximum value of the surface slope, required by the theory to be small, is about 0.4 (measured). The model underestimates the maximum slope by about 20%.

The first study of unsteady flows was the linear stability analysis described by Eqs. 22 and 23. The initial radius R_0 of the preform was taken to be 70% of the liner radius, or about 3 cm. Since the spectral properties of the glass (e.g., emissivity) depend on the absolute dimensions and temperatures rather than dimensionless ones, the results are not completely general. They are representative, however.

The critical extension ratio as a function of viscosity-temperature coupling coefficient γ is plotted in Figure 5. Computations were halted when the fiber failed to freeze before exiting the furnace. For $C_R = 50$ this point occurred at $E \approx 600$ and $\gamma \approx 8$. At smaller values of C_R cooling by radiation is less effective, and hence the faster-moving (larger extension ratio) fibers exit in the liquid state. To treat cases where the fiber freezes outside the furnace, the model would have to be modified to include convective heat transfer to the low-temperature surroundings.

The most apparent feature of Figure 5 is the stability of the preform-drawing process at values of γ greater than 10. Silica glass ($\gamma \approx 32$) drawing at large values of C_R is stable at all extension ratios. Shah and Pearson (1972) reported very similar behavior in the case of draw-down flows with convection-dominated heat transfer. Their stability boundary as a function of the viscosity-temperature coupling coefficient closely resembles the contours in Figure 5.

It is interesting to note that in the parameter range where instability can occur, an increase in C_R actually decreases stability. (The critical extension ratio is lower at fixed γ.) Shah and Pearson also noted this trend. An increase in their Stanton number, analogous to C_R, produces a decrease in stability at large values of the Stanton number. Of course, the trend must reverse as C_R becomes small enough, since E is very small (20.21) and independent of γ in the $C_R = 0$ (isothermal) limit. Geyling and Homsy (1980) have illustrated the complexity of the small C_R limit. They found with their radiation model that the stability contours were of very nonmonotonic shape, perhaps not even simply connected. This limit was not investigated here, because it is below the range of practical interest, and the assumptions of this model are not satisfied for small C_R. An investigation of the small C_R regime is an important subject for future investigation.

The results of Figure 5 were discovered empirically years ago in the preform-drawing industry, at values of γ appropriate for commercial glasses. Hence the practical value of this model lies largely in its ability to quantify other sources of diameter varia-

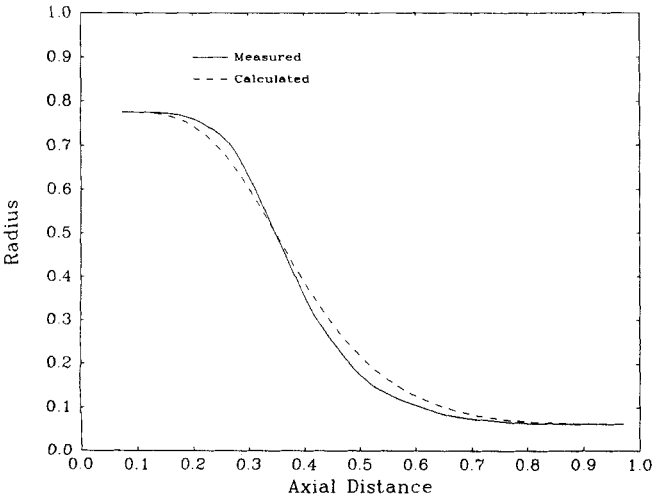

Figure 4. Mean radius profiles of drawn preform.
Radial coordinate is normalized by liner radius, axial coordinate by liner length.

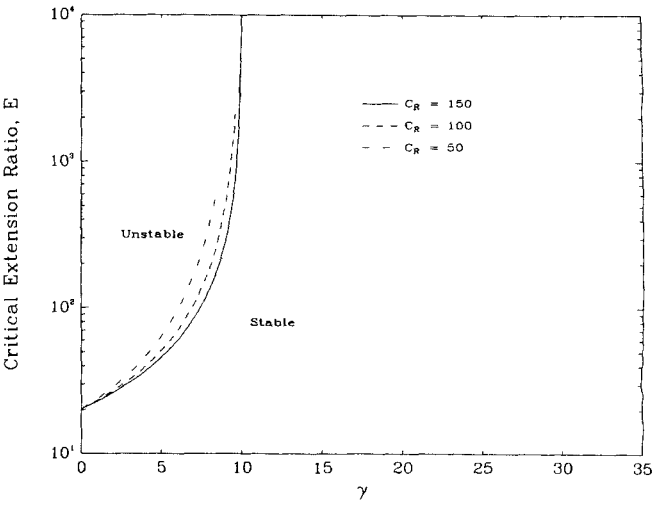

Figure 5. Critical extension ratio versus viscosity-temperature coupling coefficient.

tions. One such source is an unsteady take-up speed, which was analyzed by solving the boundary-value problem described by Eqs. 24 and 25. The final diameter variation relative to the mean diameter is given by the magnitude of the complex disturbance radius χ, evaluated at the freezing point ζ_1. The diameter variation is plotted as a function of forcing frequency in Figure 6. Because time is normalized by the very large scale L/V_0, the dimensionless frequencies considered are quite high.

Following a sharp initial drop, a slow, nearly linear decay with frequency can be seen in Figure 6. The oscillations modulating the linear decay are presently being studied; it is known however that their amplitudes depend strongly upon the furnace temperature profile. Figure 6 also demonstrates how the draw-down flow is very insensitive to unsteady take-up rates. At a dimensionless frequency of 1,000, the ratio of unsteady velocity amplitude to radius amplitude is 10, i.e., a 10% velocity variation would be required to produce a final radius perturbation of 1%.

A set of experiments was performed to experimentally evaluate the frequency response to the unsteady take-up rate. A preform of initial dimensionless radius 0.8 was elongated by an extension ratio of approximately 300. Once the process was judged to be as steady as possible, the take-up speed was deliberately varied at frequencies of 0.005, 0.01, and 0.02 Hertz. The diameter of the fiber exiting the furnace was measured by a detector and recorded on chart paper. Four cycles of the trace at 0.02 Hertz are shown in Figure 7. The chart recording was digitized and processed through a Fast Fourier Transform program, to separate the linear response at the desired frequency from nonlinear effects and preexisting oscillations at other frequencies. The experimental diameter responses are displayed on Figure 6. The theoretical value is within a factor of two of the experimental one at the low frequency, and within a factor of three at the high frequency. The theoretical values show the correct decay with frequency as measured by the experimental fall-off. The overall agreement of theory with experiment is considered to be good, in light of the difficulties inherent in quantitatively treating radiation heat transfer.

Also given in Figure 6 are values of the perturbation radius calculation using the dynamic boundary condition (Eq. 25). The

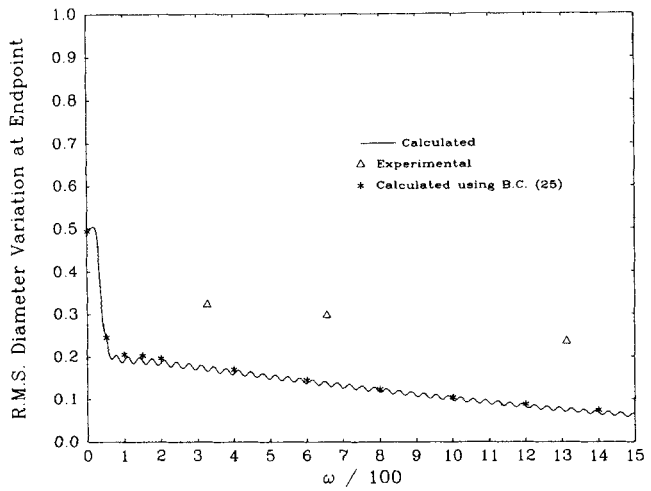

Figure 6. Diameter response to periodic take-up rate of unit amplitude as a function of frequency.
Time is nondimensionalized by the convective time scale L/V_0.

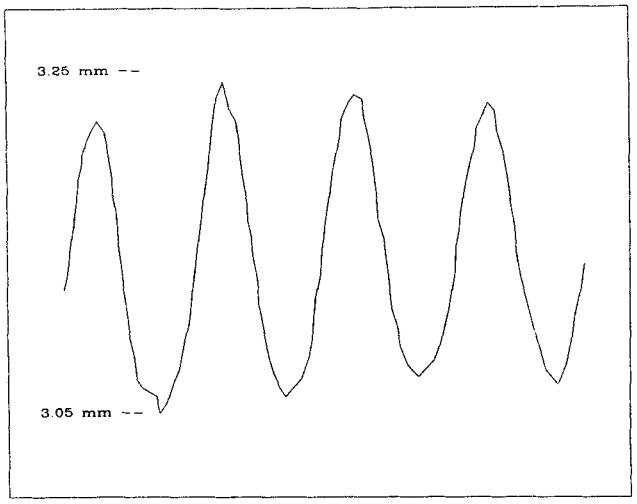

Figure 7. Experimental trace of diameter at take-up point as a function of time.
Forcing period is 50 seconds.

agreement between the two theoretical values is close at all frequencies, possibly indicating an insensitivity of the response to endpoint boundary conditions. Chang, Denn, and Kase (1982) also discovered a weak dependence upon boundary condition in the final radius perturbation. Such an insensitivity is encouraging, considering our imprecise knowledge of the equations describing solidification.

Conclusions

The theory of unsteady draw-down flows has been extended to include the case of preform drawing, in which radiative exchange with a furnace is the dominant form of heat transfer. A radiation heat transfer model was introduced which accounted for the shape of the preform surface, the spectral variation in the glass properties, and the dependence of emissivity upon fiber diameter. A set of linearized disturbance equations based upon the small-slope assumption was derived and solved subject to two separate boundary conditions. The solution to an eigenvalue problem provided a set of stability boundaries for the critical extension ratio as a function of the viscosity-temperature coupling coefficient γ, at several values of the radiation transfer coefficient C_R. At values of C_R and γ encountered in practice, the preform-drawing process was found to be extremely stable. A boundary-value problem was solved to analyze the effect of a periodic take-up rate on the final fiber diameter. The magnitude of the disturbance radius plotted against forcing frequency revealed an insensitivity of the process to fluctuations in take-up speed. The results of the boundary-value problem were found to be in good agreement with experimental values, especially in dependence upon frequency. Further insight into the sources of diameter variations can be readily obtained with the model, through consideration of different mean flows and sensitivity studies based upon other disturbances.

Acknowledgment

The support of Dan Nolan of the applied physics group is gratefully acknowledged. The author wishes also to thank Dale Powers and Mark McDermott for help with the experiments and Walt Buehl for many productive discussions.

Notation

a = absorption coefficient
b = radius of furnace liner
c_p = specific heat of glass
$C_R = (2\sigma T_s^3 L)/(\rho c_p V_0 b)$ = radiation transfer coefficient
dA_g = differential area element on glass surface
dA_w = differential area element on liner
d^2Q_a = energy radiated by dA_w which is absorbed by dA_g
$E = V_1/V_0$ = extension ratio
$e_{\lambda b}$ = blackbody hemispherical spectral emissive power
F = geometric factor for calculating radiation from liner to glass
$i'_{\lambda,w}$ = spectral intensity of radiation leaving dA_w
$\vec{i}$ = Cartesian unit vector in x-direction
$\vec{j}$ = Cartesian unit vector in y-direction
$\vec{k}$ = Cartesian unit vector in z-direction
k = thermal conductivity of glass
k_{gas} = thermal conductivity of purge gas
$k_r = (-16n^2\sigma T_s^3)/(3a)$ = "radiation conductivity"
L = length of furnace liner
n = index of refraction
$\vec{n}_g$ = unit vector normal to dA_g
$\vec{n}_w$ = unit vector normal to dA_w
Pr = Prandtl number of purge gas flow
q_a = absorbed radiation per unit area
q_c = convective heat transfer to purge gas, per unit area
q_e = emitted radiation per unit area
R = radius of glass surface
R_0 = radius of preform before draw down
Re = Reynold's number of purge gas flow
r = radial coordinate measured from z-axis
s = external heat per unit area added to liner
$\vec{S}$ = vector connecting dA_g and dA_w
S = length of $\vec{S}$
t = temporal coordinate
T = glass temperature
T_s = softening point of glass
T_w = temperature of dA_w
U = total radiated energy per unit area leaving dA_w
v_z = axial velocity of glass jet
V_0 = axial velocity of glass jet at $z = z_0$
V_1 = axial velocity of glass jet at $z = z_1$
z = axial coordinate aligned with axis of system rotation
z_0 = upper endpoint of draw-down zone
z_1 = lower endpoint of draw-down zone
z_g = axial coordinate of dA_g
z_w = axial coordinate of dA_w

Greek letters

α'_λ = directional spectral absorptivity of glass
β_g = angle between $\vec{S}$ and $\vec{n}_g$
β_w = angle between $\vec{S}$ and $\vec{n}_w$
γ = viscosity-temperature coupling coefficient
ΔT_r = representative temperature difference between glass surface and liner
ΔT_z = difference between maximum liner temperature and T_s
ϵ'_λ = directional spectral emissivity of glass
ϵ_λ = hemispherical spectral emissivity of glass
ϵ_w = emissivity of liner (assumed to be a diffuse, gray reflector)
$\mathrm{E} = b/L$ = slenderness ratio of glass jet
$\zeta = z/L$ = dimensionless axial coordinate
$\zeta_0 = z_0/L$ = dimensionless upper endpoint of draw-down zone
$\zeta_1 = z_1/L$ = dimensionless lower endpoint of draw-down zone
$\eta = \mu/\mu(T_s)$ = dimensionless viscosity
θ = dimensionless mean glass temperature
θ' = dimensionless disturbance glass temperature
$\theta_r(\zeta) + i\theta_i(\zeta)$ = complex amplitude in normal-mode decomposition of disturbance temperature
λ = wavelength of radiation
μ = glass viscosity
$\xi = 14{,}388\ \mu\mathrm{m} \cdot \mathrm{K}/(\lambda T)$
ρ = glass density
σ = Stefan-Boltzman constant
$\tau = V_0 t/L$ = dimensionless temporal coordinate
$\phi_a = q_a/(\sigma T_s^4)$ = dimensionless absorbed radiation
$\phi_e = q_e/(\sigma T_s^4)$ = dimensionless emitted radiation
φ = polar coordinate
φ_w = polar coordinate of dA_w
φ_0 = value of φ_w at which $\cos\beta_w = 0$
$\bar{\chi}$ = dimensionless mean radius of glass surface
χ' = disturbance radius of glass surface
$\overline{\chi_0} = R_0/b$ = dimensionless radius of preform before draw-down
$\chi_r(\zeta) + i\chi_i(\zeta)$ = complex amplitude in normal-mode decomposition of disturbance radius
$\bar{\psi}$ = dimensionless mean velocity of glass jet
ψ' = disturbance velocity of glass jet
$\psi_r(\zeta) + i\psi_i(\zeta)$ = complex amplitude in normal-mode decomposition of disturbance velocity
$\omega_r + i\omega_i$ = complex growth rate of normal modes in stability analysis
ω = disturbance frequency in unsteady boundary-value problem

Literature Cited

Chang, J. C., M. M. Denn, and S. Kase, "Dynamic Simulation of Low-Speed Melt Spinning," *Ind. Eng. Chem. Fund.*, **21**(1), 13 (1982).

Denn, M. M., "Continuous Drawing of Liquids to Form Fibers," *Ann. Rev. Fluid Mech.*, **12**, 365 (1980).

Fisher, R. J., and M. M. Denn, "Finite-Amplitude Stability and Draw Resonance in Isothermal Melt Spinning," *Chem. Eng. Sci.*, **30**, 1129 (1975).

———, "Mechanics of Nonisothermal Polymer Melt Spinning," *AIChE J.*, **23**(1), 23 (1977).

Gelder, D., "The Stability of Fiber Drawing Processes," *Ind. Eng. Chem. Fund.*, **10**(3), 534 (1971).

Geyling, F. T., and G. M. Homsy, "Extensional Instabilities of the Glass Fiber Drawing Process," *Glass Tech.*, **21**(2), 95 (1980).

Gardon, R., "The Emissivity of Transparent Materials," *J. Amer. Ceram. Soc.*, **39**(8), 278 (1956).

Glicksman, L. R., "The Dynamics of a Heated Free Jet of Variable Viscosity Liquid at Low Reynolds Numbers," *J. Basic Eng., Trans. ASME*, **90**, 343 (1968).

Ishihara, H., and S. Kase, "Studies on Melt Spinning. V. Draw Resonance as a Limit Cycle," *J. Appl. Polym. Sci.*, **19**, 557 (1975).

Kase, S., "Studies on Melt Spinning: IV. On the Stability of Melt Spinning," *J. Appl. Polym. Sci.*, **18**, 3279 (1974).

Kase, S., and M. Araki, "Studies on Melt Spinning: VIII. Transfer Function Approach," *J. Appl. Polym. Sci.*, **27**, 4439 (1982).

Kase, S., and T. Matsuo, "Studies on Melt Spinning. I. Fundamental Equations on the Dynamics of Melt Spinning," *J. Polym. Sci.*, **A3**, 2541 (1965).

———, "Studies on Melt Spinning: II. Steady-State and Transient Solutions of Fundamental Equations Compared with Experimental Results," *J. Appl. Polym. Sci.*, **11**, 251 (1967).

Mhaskar, R. D., and Y. T. Shah, "Stability Analysis of Glass Fiber Spinning," *Glass Tech.*, **18**(5), 152 (1977).

Paek, U. C., and R. B. Runk, "Physical Behavior of the Neck-Down Region During Furnace Drawing of Silica Fibers," *J. Appl. Phys.*, **49**(8), 4417 (1978).

Pearson, J. R. A., and M. A. Matovich, "On the Spinning of a Molten Threadline: Stability," *Ind. Eng. Chem. Fund.*, **8**(4), 605 (1969).

Pearson, J. R. A., and Y. T. Shah, "On the Stability of Isothermal and Nonisothermal Fiber Spinning of Power-Law Fluids," *Ind. Eng. Chem. Fund.*, **13**(2), 134 (1974).

Pearson, J. R. A., Y. T. Shah, and R. D. Mhaskar, "On the Stability of Fiber Spinning of Freezing Fluids," *Ind. Eng. Chem. Fund.*, **15**(1), 31 (1976).

Petrie, C. J. S., and M. M. Denn, "Instabilities in Polymer Processing," *AIChE J.*, **22**(2), 209 (1976).

Sayles, R., and B. Caswell, "A Finite Element Analysis of the Upper Jet Region of a Fiber Drawing Flow Field," National Science Foundation NSF-18421/1 (1981).

Schultz, W. W., and S. H. Davis, "One-Dimensional Liquid Fibers," *J. of Rheol.*, **26**(4), 331 (1982).
Schultz, W. W., A. Zebib, S. H. Davis, and Y. Lee, "Nonlinear Stability of Newtonian Fibers," *J. Fluid Mech.*, **149**, 455 (1984).
Shah, Y. T., and J. R. A. Pearson, "On the Stability of Nonisothermal Fiber Spinning," *Ind. Eng. Chem. Fund.*, **11**(2), 145 (1972a).
———, "On the Stability of Nonisothermal Fiber Spinning—General Case," *Ind. Eng. Chem. Fund.*, **11**(2), 150 (1972b).
Siegel, R., and J. R. Howell, *Thermal Radiation Heat Transfer*, McGraw-Hill, New York (1981).
Usiskin, C. M., and R. Siegel, "Thermal Radiation from a Cylindrical Enclosure with Specified Wall Heat Flux," *J. Heat Transf. Trans. ASME*, **82**(4) 369 (1960).
Young, D. G., and M. M. Denn, "Disturbance Propagation in Melt Spinning," *Chem. Eng. Sci.*, accepted (1988).

Appendix A

In this appendix the temperature and radiative flux for a cylindrical enclosure are calculated from theoretical considerations, using the method of Usiskin and Siegel (1960). The temperature is assumed to be high enough that heat-transfer modes other than radiation are unimportant.

Consider a hollow cylinder of radius b and length L which is heated from the outside by a source $s(z)$. The environment temperature at each end of the cylinder is T_e. Usiskin and Siegel showed that the total radiation flux leaving the surface is

$$U(z) = \sigma T_e^4 + \Gamma(z), \tag{A1}$$

where $\Gamma(z)$ solve the integral equation

$$\Gamma(z) = s(z) + \int_0^z \Gamma(\eta)K(z-\eta)\,d\eta + \int_z^L \Gamma(\eta)K(\eta - z)\,d\eta \tag{A2}$$

with

$$K(x) = 1 - \frac{x^3 + 3x/2}{(x^2+1)^{3/2}}. \tag{A3}$$

The wall temperature T_w is obtained from the relation

$$\sigma T_w^4(z) = \frac{1-\epsilon_w}{\epsilon_w} s(z) + U(z), \tag{A4}$$

ϵ_w being the emissivity of the liner. The liner is assumed to be a diffuse gray reflector.

A conventional induction furnace liner was modeled by taking s to be constant over part of the length and zero elsewhere. Specifically, the fraction between $z = 0.5$ and $z = 3$ diameters is heated. The length of the liner is 5 of its diameters. The environment temperature was taken to be one-seventh the softening point of the glass. The magnitude of the constant heat flux was not known, however, it was assumed that the maximum furnace temperature was 1.17 times the softening point. For silica glass this corresponds to a maximum temperature of 2,000°C based upon a softening point of 1,667°C.

Equation (A2) was solved by the method of successive approximations, startng from an initial guess for $\Gamma(z)$ in the form of a parabola. Roughly 100 iterations were required to achieve an average (over an 80 point grid) relative error of 10^{-5}. Approximately 10 minutes of CPU time (on a VAX 8800) was required. By normalizing Γ with the magnitude of $s(z)$, it was necessary to solve Eq. A2 only once to determine the heat flux necessary for attaining the desired maximum temperature.

The profile $T_w(z)$ was shown to the right in Figure 1.

Appendix B

In this appendix we evaluate the geometric factor

$$F = \frac{b}{\pi}\int_{\varphi_0}^{\pi-\varphi_0} \frac{\cos\beta_g \cos\beta_w\, d\varphi_w}{S^2} \tag{B1}$$

appearing in the expression for the absorbed radiation. The various quantities in the integrand are defined as follows.

Consider a differential element dA_w located on the wall, having cylindrical coordinates $(r, \varphi, z) = (b, \varphi_w, z_w)$, and an element dA_g on the surface of the glass with coordinates $(R, \pi/2, z_g)$. Due to rotational symmetry the polar coordinate of dA_g is unimportant; we take it to be $\pi/2$ (where the x-axis represents $\varphi = 0$) for convenience. The normals to dA_g and dA_w are

$$\vec{n}_g = \frac{\vec{j} - \frac{dR}{dz}\vec{k}}{\left[1 + \left(\frac{dR}{dz}\right)^2\right]^{1/2}}$$

and

$$\vec{n}_w = -\cos\varphi_w\vec{i} - \sin\varphi_w\vec{j},$$

where $\vec{i}, \vec{j}$, and $\vec{k}$ are the standard Cartesian unit vectors for a coordinate system in which draw down takes place along the positive z-axis. The cosines of the angles between the normals and the vector connecting dA_g and dA_w are

$$\cos\beta_g = \frac{b\sin\varphi_w - R - \frac{dR}{dz}(z_w - z_g)}{\left[1 + \left(\frac{dR}{dz}\right)^2\right]^{1/2} S}$$

and

$$\cos\beta_w = \frac{b - R\sin\varphi_w}{S},$$

where

$$S = [b^2\cos^2\varphi_w + (R - b\sin\varphi_w)^2 + (z_w - z_g)^2]^{1/2}$$

is the distance separating the two area elements. The limits of integration represent the angles at which dA_g can no longer see dA_w, i.e., where $\cos\beta_g = 0$:

$$b\sin\varphi_0 - R - \frac{dR}{dz}(z_w - z_g) = 0. \tag{B2}$$

Due to even symmetry about $\varphi_w = \pi/2$, the integral from φ_0 to $\pi/2$ can be doubled. Expression B1 becomes

$$F = \frac{2/(\pi b)}{\sqrt{1 + \left(\frac{dR}{dz}\right)^2}} \int_{\varphi_0}^{\pi/2} d\varphi_w \frac{-2\frac{R}{b} - \frac{dR}{dz}\frac{z_w - z_g}{b} + \frac{R}{b}\cos^2\varphi_w + \sin\varphi_w\left(1 + \frac{R^2}{b^2} + \frac{dR}{dz}\frac{z_w - z_g}{b}\frac{R}{b}\right)}{\left[1 + \frac{R^2}{b^2} - 2\frac{R}{b}\sin\varphi_w + \left(\frac{z_w - z_g}{b}\right)^2\right]^2} \tag{B3}$$

Standard techniques can be used to perform the integration in Eq. B3. The result is

$$F = \frac{2/(b\pi)}{\left[1 + \left(\frac{dR}{dz}\right)^2\right]^{1/2}}\left[\left(\frac{1}{2} + \frac{C_1C_4 - C_3C_2}{D^2}\right)\frac{\cos x}{C_3 + C_4\sin x} + \frac{x}{2C_4} + \frac{2(C_1C_3 - C_2C_4) - \frac{C_3}{C_4}D^2}{D^3} \cdot \arctan\frac{C_3\tan\frac{x}{2} + C_4}{D}\right]_{\varphi 0}^{\pi/2}, \tag{B4a}$$

where

$$C_1 = -2\frac{R}{b} - \frac{dR}{dz}\frac{z_w - z_g}{b} \tag{B4b}$$

$$C_2 = 1 + \frac{R^2}{b^2} + \frac{R}{b}\frac{dR}{dz}\frac{z_w - z_g}{b} \tag{B4c}$$

$$C_3 = 1 + \frac{R^2}{b^2} + \left(\frac{z_w - z_g}{b}\right)^2 \tag{B4d}$$

$$C_4 = -2\frac{R}{b} \tag{B4e}$$

$$D^2 = C_3^2 - C_4^2. \tag{B4f}$$

To the level of accuracy retained in the energy equation, terms containing dR/dz or its square may be neglected under the small-slope approximation. The slope is multiplied by the potentially large factor $(z_w - z_g)/b$, however, in these cases $(z_w - z_g)/b$ also appears raised to negative fourth power. The entire term is then extremely small when $(z_w - z_g)$ is much larger than b. (The physical statement is that most of the heat comes from the part of the furnace directly opposite the observation point.) The absence of the $(dR/dz)[(z_w - z_g)/b]$ terms produces a significant simplification in the disturbance equations.

Manuscript received Aug. 17, 1988, and revision received Dec. 19, 1988.